Proceedings of the ASME 2014 International Mechanical Engineering Congress and Exposition
IMECE2014
November 14-20, 2014, Montreal, Quebec, Canada

IMECE2014-39286

Experimental, Numerical and Analytical Investigation of Thermal Resistance in High Brightness LED Arrays

[1]Mahmood R.S Shirazy, [1]Andréane D'Arcy-Lepage, [2]Michel Gilbert, [2]Samuel Richard, [1]Luc G. Fréchette
[1]Department of Mechanical engineering, Université de Sherbrooke, Sherbrooke, Qc, Canada,
[2]LEDTECH, Sherbrooke, Qc, Canada

ABSTRACT

Thermal performance of a commercial LED array module has been studied by experimental, numerical and analytical approaches to find the dominant thermal resistance in the thermal circuit. The light quality, lifetime and reliability of the LED modules depend strongly on the junction temperature which can be obtained and modified by a suitable thermal resistance model. Analytical models for the first level packaging (Die) and second level packaging (PCB and heat sink) have been developed with special attention to the thermal spreading resistance. Numerical modeling has been performed using commercial finite element software (COMSOL) and the results are in good agreement with the analytical models. An LED array module has also been studied experimentally by measuring the temperature field in the PCB and heat sink using thermocouples and infrared thermography. The results of the experimental part are used to validate the numerical and analytical models. It is shown that more than 50% of the total thermal resistance is caused by the heat sink while the PCB and LED package each share 25% of the total thermal resistance.

INTRODUCTION

Light-emitting diodes (LEDs) are replacing more and more other lighting technologies such as incandescent, fluorescent and halogen types. The drive for this trend stems from their outstanding properties such as small size, low power consumption, high brightness and long operating life. LEDs consist of a semiconductor chip with a p-n junction diode [1]. When a current is applied, electrons and holes from different electrodes recombine in the junction either radiatively or nonradiatively. The radiative recombination will emit photons (light) but the nonradiative process will result in a self-heating process. This nonradiative recombination process along with Joule heating at the diode and interconnects are the main heat sources in the LED package. The generated heat should be evacuated because otherwise it will increase the junction temperature. High junction temperatures can lead to lower light output, LED color shift and decreased lifetime. A typical high brightness (HB) LED chip has $1mm^2$ surface area with a total power consumption of 1W [2]. Currently, the LEDs on the market have a luminous efficiency of about 10%-30% and consequently 90% -70% of the input electrical energy is converted to heat [3]. With this efficiency, the heat flux can be as high as 80 W/cm^2 and is expected to increase to 350 W/cm^2 in the future years [4]. Therefore, LED packaging plays a critical role in effective thermal management to achieve a junction temperature below a maximum value of typically 140-150 ^oC.

As can be seen in Figure 1, a LED module is typically composed of a LED package mounted on a printed circuit board (PCB) and a heat sink to transfer the heat to the ambient. The LED package consists of die, die attach, heat conducting slug enclosed in a ceramic package, thermal slug pad, encapsulation and lens. Electrical connections are established through the lead frames to the copper layers but are not shown here because their thermal contribution is negligible [5]. The PCB shown here is a metal core type (MC PCB) and consists of a dielectric insulator layer on top of the anodized aluminum [6]. The copper layers are the electrical conductors to transport electricity between LEDs in the arrays (not shown). The MC PCB is mounted on an aluminum heat sink which is exposed to the ambient.

The heat is generated in the LED die (at the junction) and the highest temperature is therefore the junction temperature. Heat can be transported to the ambient through two paths. One is by conduction through the encapsulation and the lens around the die while the other is by conduction through the LED package, the PCB and the heat sink. Although in the both paths the final thermal sink is the ambient, the first path is often not accessible because the LEDs might be covered by a plastic lid for protection and light enhancement. In addition to preventing natural convection form the PCB surface, the plastic lid is often opaque to infrared radiation and hence blocks the thermal radiation from the PCB surface to the ambient. Moreover, thermal conductivity of the encapsulation and the lens are much lower than that of the heat slug under the die. Therefore, conduction through the die backside is often the main heat transfer path. The total thermal resistance between the junction and the ambient is:

$$R_{Total} = R_{LED\ package} + R_{PCB} + R_{Heat\ sink} \quad (1)$$

The overall thermal resistance can also be expressed as:

$$R_{total} = \frac{T_{Die} - T_{Ambient}}{Q_{LED}} \quad (2)$$

where T_{Die} and $T_{Ambient}$ are die and ambient temperatures and Q_{LED} is the LED input power converted to heat (W). Hence, the die temperature (junction temperature) can be decreased either by decreasing the LED power, ambient temperature or the module total thermal resistance. While the LED input power and ambient temperature are constrained by the application, the module total thermal resistance can be modified through different design parameters to minimize the junction temperature.

Junction temperature of LED arrays can be determined either experimentally, numerically or analytically. Experimental techniques such as IR thermography at the junction level [7, 8], peak wavelength shift [9] and forward voltage measurement [10, 11] are used to measure the junction temperature. These methods can characterize the thermal performance of the LED arrays under different operating conditions. However, they lack the flexibility for parametric studies and are not useful during the thermal design process. Numerical simulations are also used extensively to obtain the junction temperature and the thermal performance of the LED modules [12-14]. Although relatively easy to implement, the disadvantage of the numerical approach is that to obtain a precise value for the junction temperature, the complete data regarding the material and dimensions of the LED package, PCB and heat sink should be available. In the case of the LED package, this data is not usually available to the light module designer. However, the thermal resistance of the commercial LED packages is usually provided by the LED manufacturers. Moreover, numerical studies can be very time consuming for parametric studies. Analytical approaches on the other hand, are very appealing because they are readily suitable for parametric studies and variable conditions.

LED arrays basically form a conduction problem with multi heat source on a multilayer substrate. Thus spreading thermal resistance is typically significant when heat transfers from the LED die through the PCB and eventually the heat sink [15]. More complexity arises when considering the effect of multiple heat sources on a PCB and heat sink. Few analytical solutions for the temperature field of the LED array [16-18] and LED module thermal resistance [19, 20] are already available. In most cases, numerical solutions are used to validate the analytical results and no experimental validation is presented.

This work therefore aims to present an analytical thermal model for a LED module along with its experimental validation. A commercial LED module including 30 LED packages attached on a MC PCB and a heat sink were investigated. Temperature measurement was performed by using thermocouples and infrared thermography. Temperature profile on the PCB surface was obtained and the results are compared with the numerical and analytical results. The contribution of each component (LED package, PCB and heat sink) to the total thermal resistance will also be presented. The analytical model includes spreading thermal resistance in the multi-layer PCB and multi-heat source heat sink. This model therefore provides a powerful tool for parametric studies and thermal design efforts of the LED modules.

EXPERIMENTAL METHODS

Geometrical and thermal properties of the LED module

Part of a LED module is shown in Figure 1. The LED die is made by Bridgelux™ and has 1W power and a luminous efficiency of 15% (85% of the power is therefore converted to heat). The LED package is fabricated by a third party manufacturer and the thermal resistance as provided by the manufacturer is 12 °C/W. Table 1 shows the dimensions and thermal properties of the LED module components. It should be noted that while the dimensions can be measured readily, it is more difficult to identify the exact materials and their corresponding thermal conductivities especially for LED package. Numerical simulations show that LED package thermal resistance is most sensitive to the die and die attach thermal conductivities. The choice of the material for these components can significantly affect the LED package thermal resistance.

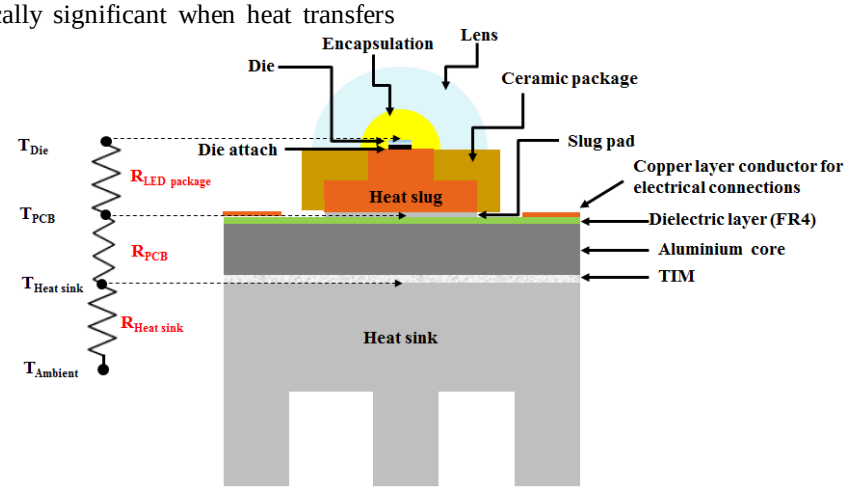

Figure 1. Typical LED module including LED package, board (PCB) and heat sink.

Table 1 Dimensions and material properties of the LED package

Part	Dimensions (mm)	Material	Thermal conductivity, k (W/m K)
Lens	Diameter: 6	Polycarbonate [5]	0.2
Encapsulation	-	Silicone gel [5]	0.2
Die	1.1×1.1×0.15	Aluminium oxide [22]	30
Die attach	1.1×1.1×0.15	Silver epoxy [21]	6
Heat slug	O.D.: 5.5 Height: 0.8 I.D.: 3 Height: 1.9	Copper	385
Slug pad	Diameter: 5.5 Height: 0.05	Thermally conductive epoxy [5]	5
Ceramic package	Diameter: 8 Height: 2.7	Ceramic [5]	4.5
Copper layer conductor	First and last layer : 18×64×0.08 Middle layers: 15×64×0.08	Copper	385
Dielectric	270×64×0.08	FR4 [23]	0.3
Metal core	270×64×1.6	Aluminium	160
TIM	270×64×0.05	Thermal epoxy [5]	5
Heat sink	Number of fins: 19	Aluminium	160

Thermal conductivity of the die material is provided by the manufacturer. As for the die attach, silver epoxies have a thermal conductivity from 2 to 12 W/m K [21]. Numerical simulation of a single LED package shows that by using a die attach thermal conductivity of 6 W/m K, the thermal resistance of the LED package will be the same as the value provided by the manufacturer. Typical values of thermal conductivity are used for all other components. LED packages are attached by soldering to a MC PCB in a 10×3 array of LEDs. Figure 2a shows half of the MC PCB (the soldering connections are not shown). MC PCB is composed of an aluminium core, a dielectric layer (FR4) and copper strips for electrical connections. Although not shown here but the entire MC PCB surface is covered by very thin (~10μm) white coating. While its thermal resistance can be neglected due to its extremely small thickness, it will lead to a uniform surface emissivity which is suitable for IR thermography. Figure 2b shows the LED package locations on the MC PCB. The MC PCB is attached by a thermal epoxy to an aluminum heat sink (Figure 2c).

Three type-K thermocouples (OMEGA®, 0.25 mm diameter tip) are used to measure the temperature at three different locations on the MC PCB. Two of the thermocouples, T1 and T2 are shown in Figure 2b. T3 was placed at the same location of T2 but on the opposite side of the MC PCB surface (not shown here). The thermocouples were connected to a data acquisition system (Agilent® 34970A). A high performance IR camera (Flir® SC620) with a resolution of 640×480 pixels was used to capture the temperature profile on the MC PCB. By comparing the temperatures obtained by the thermocouples and the IR camera, the MC PCB surface emissivity was estimated to be 0.89.

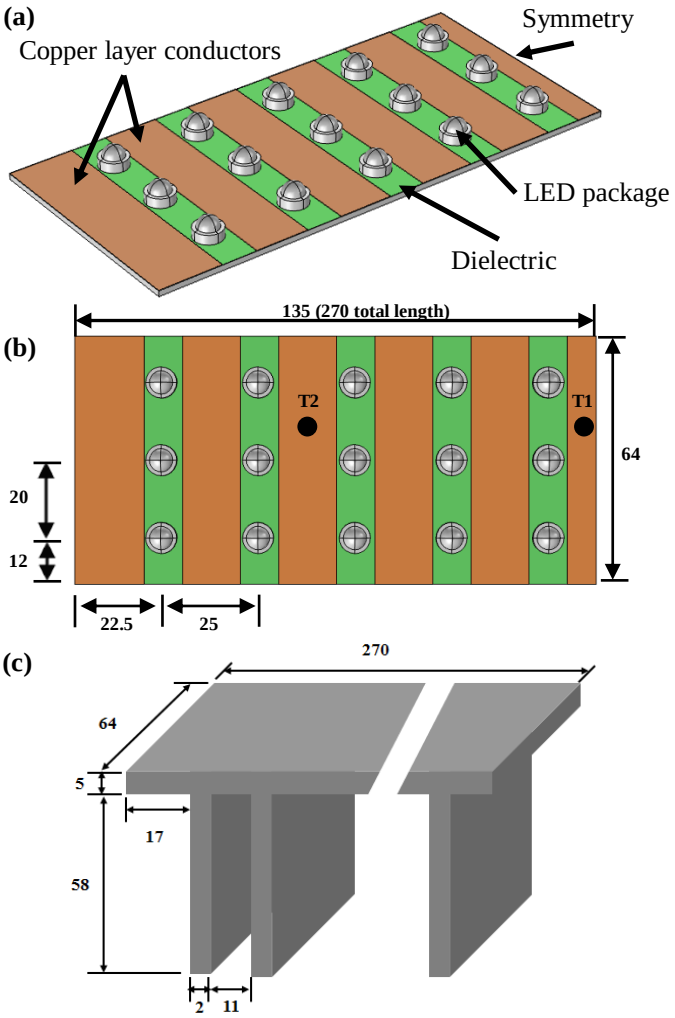

Figure 2. a) Schematic drawing of half of the MC PCB with 5×3 LED packages b) LED package locations on the MC PCB along with locations of the two of the thermocouples c) heat sink (dimensions in mm).

Test procedures

To evaluate the impact of each LED module component, experimental measurements were performed separately on a complete LED module (including LED packages, MC PCB and heat sink), LED module without the heat sink and then only the heat sink. The top surface of the commercial module was covered by a plastic lid which was opaque to the infrared radiation and hence, rendering the IR thermography impossible. The complete module and the module without the heat sink were tested by running the LEDs for 20 mins until the temperatures on the MC PCB surface measured by thermocouples were stable. The temperature was measured in

2s intervals by the attached thermocouples. Then, the plastic lid was removed temporarily and the temperature profile was captured by the IR camera. The short time required to take the IR image showed no meaningful impact on the temperatures measured by the thermocouples. Therefore, the experimental error caused by this method is negligible. The IR images are then processed by the specialized software FLIR ResearchIR® to obtain the temperature profiles on different locations.

The heat sink was also tested to obtain the average effective convection heat transfer coefficient. To perform this test, MC PCB was removed and a kapton® heater with the same width as the heat sink was attached on the heat sink (Figure 3). The heater surface and the uncovered top of the heat sink were covered by a thermal insulation to minimize the heat loss by convection from the top surface. Four type-K thermocouples (OMEGA®, 0.25 mm diameter tip) were used to measure the temperature at the base and tip of the central fins each with two thermocouples. The central fins were selected to minimize the spreading thermal resistance along the heat sink base plate. After turning on the heater, the steady state temperature profile was achieved after 45mins and the measured temperatures were averaged over the last 2mins of the acquired steady state data. IR camera was used to capture the heat sink temperature profile. The same surface emissivity as the MC PCB (0.89) was obtained by comparing the IR images and the temperatures measured by the thermocouples. These data along with the measured ambient temperature were used to calculate the average effective convection heat transfer coefficient of the heat sink due to both radiation and natural convection.

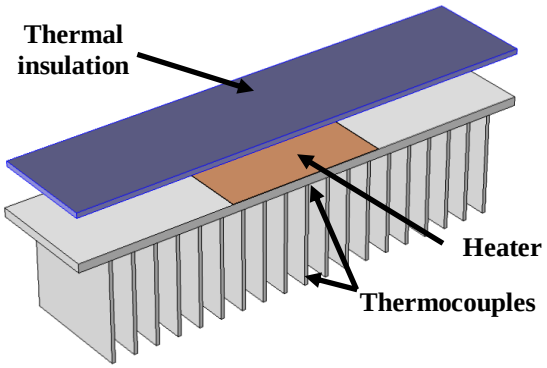

Figure 3. Schematic drawing of the heat sink test setup to measure the effective convection heat transfer coefficient.

GOVERNING EQUATIONS AND MODELS

Configuration and assumptions for analytical models

Figure 4 shows the simplified configuration of the LED module with its corresponding boundary conditions. Comparing this configuration with Figure 1 shows that some components of the LED module are ignored to simplify the geometry. In the LED package, the lens, encapsulation and ceramic package are ignored due to their very low thermal conductivities. A uniform heat flux is applied at the die surface. Moreover, spreading thermal resistance due to variable cross sections between the die attach and the heat slug and also between the two parts of the heat slug are also ignored. This hypothesis is valid due to high thermal conductivity of the copper heat slug and its small dimensions. In the MC PCB, heat is transferred from back side of the LED package. It can be seen that the copper layer conductors for the electrical connections are also ignored. Numerical simulations show that the effect of this copper layer in the heat transfer is negligible due to very low thermal conductivity of the dielectric layer.

Heat generation in the LED die is considered as a uniform heat flux at the die surface. A uniform heat flux is also assumed on top of the MC PCB and under LED package which is shown to be a valid assumption [19]. In the analytical models, two different boundary conditions are assumed for the boundary between the TIM and the heat sink. For the MC PCB thermal resistance model, a uniform temperature is assumed at the bottom of TIM. Numerical simulations show that the temperature variations at the bottom of the TIM are very small and this assumption is therefore satisfactory. When calculating heat sink thermal resistance though, a uniform heat flux on the surface was used.

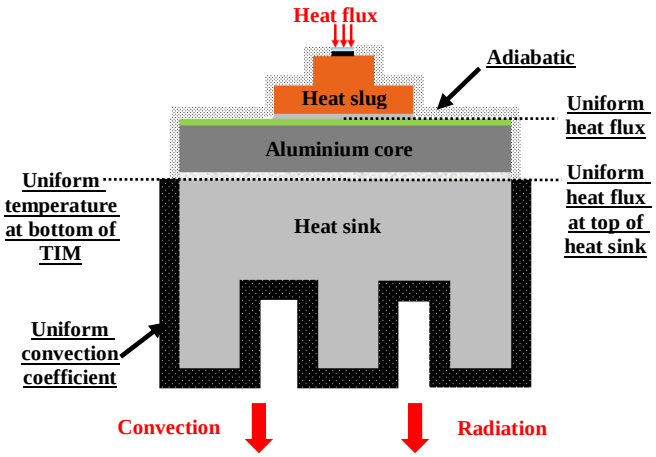

Figure 4 Simplified LED module configurations and thermal modeling assumptions

All external surfaces are assumed to be adiabatic except for the heat sink surface. Due to high surface emissivity of the heat sink (0.89), radiation mode contributes to the heat transfer as well as the natural convection, and should be taken into account. A uniform effective heat transfer coefficient is assumed on the heat sink surface that includes both convection and radiation.

Analytical model for LED package

Figure 5 shows the simplified geometry of the LED package and its thermal circuit. Ignoring the spreading thermal resistance, the thermal circuit of the LED package can be expressed using a simple1-D conduction model:

$$R_{Die} = \frac{t_{Die}}{k_{Die} A_{Die}} \tag{3}$$

$$R_{Die\ attach} = \frac{t_{Die\ attach}}{k_{Die\ attach} A_{Die\ attach}} \tag{4}$$

$$R_{Heat\ slug} = \sum_{i=1}^{2} \frac{t_{Heat\ slug,i}}{k_{Heat\ slug,i} A_{Heat\ slug,i}} \tag{5}$$

$$R_{Slug\ pad} = \frac{t_{Slug\ pad}}{k_{Slug\ pad} A_{Slug\ pad}} \tag{6}$$

$$R_{LED\ package} = R_{Die} + R_{Die\ attach} + R_{Heat\ slug} + R_{Slug\ pad} \quad (7)$$

where t, k and A are thickness (m), thermal conductivity (W/m K) and area (m^2) respectively.

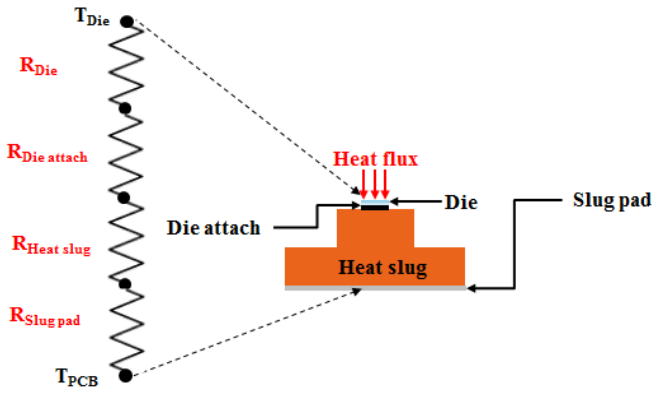

Figure 5 Schematic drawing of the simplified geometry for the LED package.

Analytical model for MC PCB

Unlike in the LED package, spreading thermal resistance cannot be ignored in the MC PCB due to very low thermal conductivity of the dielectric material. Exact analytical solution of a four layer structure with circular disks is used to obtain the MC PCB thermal resistance [19]. Circular disks are used instead of rectangular disks because the problem is simplified into a two dimensional problem due to circular symmetry (Figure 6). The simplified configuration of the MC PCB includes three layers (dielectric, aluminum core and TIM) while this model is developed for four layers. A fourth layer is added to the current configuration by dividing the dielectric layer thickness into two equal layers and hence four layers (dielectric, dielectric, aluminum and TIM) are used.

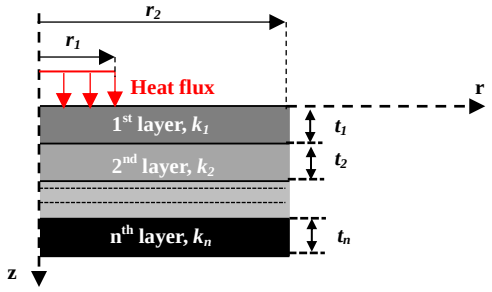

Figure 6. Multilayer circular disc geometry for MC PCB thermal modeling.

Using this model, the expression for thermal resistance is [19]:

$$R_{multi-layer} = \frac{1}{\pi r_2^2}\left(\sum_{i=1}^{n}\frac{t_i}{k_i}\right) + \frac{2}{k_1 \pi r_1}\sum_{i=1}^{\infty}\frac{J_1\left(\frac{r_1}{r_2}\alpha_l\right)}{\alpha_l^2 J_0^2(\alpha_l)}\varphi_n \quad (8)$$

where α_l is the roots of the zero-order Bessel function $J_0(x)$. The summation is performed over ascending values of α_l using Stokes approximation. A modified Stokes approximation is:

$$\alpha_l = \frac{\beta_l}{4}\left(1 - \frac{6}{\beta_l^2} + \frac{6}{\beta_l^4} - \frac{4716}{5\beta_l^4} + \frac{3902.418}{70\beta_l^4}\right) \quad (9)$$

where $\beta_l = \pi(4l+1)$ and $l \geq 1$. φ_n depends on the total number of layers and for a four layer structure is given by:

$$\varphi_4 = \frac{\left[\begin{array}{l}\frac{\tanh(t_1\lambda_l)}{k_1} + \frac{\tanh(t_2\lambda_l)}{k_2} + \frac{\tanh(t_3\lambda_l)}{k_3} + \frac{\tanh(t_4\lambda_l)}{k_4} \\ + \frac{k_2}{k_1 k_3}\tanh(t_1\lambda_l)\tanh(t_2\lambda_l)\tanh(t_3\lambda_l) \\ + \frac{k_2}{k_1 k_4}\tanh(t_1\lambda_l)\tanh(t_2\lambda_l)\tanh(t_4\lambda_l) \\ + \frac{k_3}{k_1 k_4}\tanh(t_1\lambda_l)\tanh(t_3\lambda_l)\tanh(t_4\lambda_l) \\ + \frac{k_3}{k_2 k_4}\tanh(t_2\lambda_l)\tanh(t_3\lambda_l)\tanh(t_4\lambda_l)\end{array}\right]}{\left[\begin{array}{l}\frac{1}{k_1} + \frac{\tanh(t_1\lambda_l)\tanh(t_2\lambda_l)}{k_2} + \frac{\tanh(t_1\lambda_l)\tanh(t_3\lambda_l)}{k_3} \\ + \frac{\tanh(t_1\lambda_l)\tanh(t_4\lambda_l)}{k_4} + \frac{k_2}{k_1 k_3}\tanh(t_2\lambda_l)\tanh(t_3\lambda_l) \\ + \frac{k_2}{k_1 k_4}\tanh(t_2\lambda_l)\tanh(t_4\lambda_l) \\ + \frac{k_3}{k_1 k_4}\tanh(t_3\lambda_l)\tanh(t_4\lambda_l) \\ + \frac{k_3}{k_2 k_4}\tanh(t_1\lambda_l)\tanh(t_2\lambda_l)\tanh(t_3\lambda_l)\tanh(t_4\lambda_l)\end{array}\right]} \quad (10)$$

where $\lambda_l = \alpha_l / r_2$. By using this model for the MC PCB thermal resistance, maximum temperature of the MC PCB top surface at the center will be obtained.

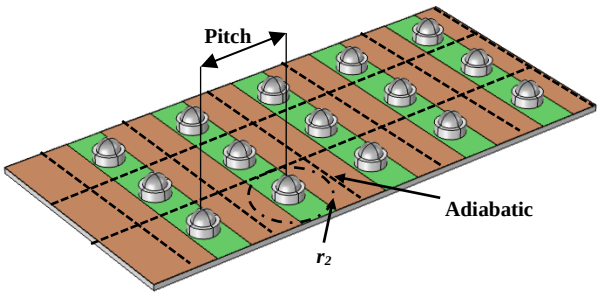

Figure 7 Schematic drawing of the MC PCB with LEDs attached with different pitches in the x and y direction.

While r_1 is radius of the heat flux area (LED package base) and is readily known, r_2 is the radius of the MC PCB surface available for the heat transfer which depends on the LED array pitch. When LED arrays are placed with a uniform distance, the distance between each LED package center is called pitch (Figure 7). This value can be different in the longitudinal or transversal directions. If all the LED packages have the same

electrical power, then the mid-surface between the LEDs can be assumed adiabatic. Therefore, r_2 can be defined as:

$$r_2 = \frac{Pitch_{\min}}{\sqrt{\pi}} \tag{11}$$

where $Pitch_{min}$ is the minimum pitch between the longitudinal and transversal directions.

Analytical model for heat sink

Thermal spreading resistance of a heat sink can be calculated by assuming N discrete heat sources each producing a heat flow of Q_i [24]. The temperature distribution on the top surface of heat sink can be obtained by:

$$T(x,y,0) - T_{Ambient} = \sum_{n=1}^{\infty} \theta_i(x,y,0) \tag{12}$$

and

$$\theta_i(x,y,0) = A_0^i + \sum_{m=1}^{\infty} A_m^i \cos(\lambda x) + \sum_{n=1}^{\infty} A_n^i \cos(\delta y) + \sum_{m=1}^{\infty}\sum_{n=1}^{\infty} A_{mn}^i \cos(\lambda x)\cos(\delta y) \tag{13}$$

where

$$A_0^i = \frac{Q_i}{ab}\left(\frac{t_1}{k_1} + \frac{1}{h_{eff}}\right) \tag{14}$$

$$A_m^i = \frac{2Q_i\left[\sin\left(\frac{(2x_i + c_i)}{2}\lambda_m\right) - \sin\left(\frac{(2x_i - c_i)}{2}\lambda_m\right)\right]}{abc_i k_1 \lambda_m^2 \phi(\lambda_m)} \tag{15}$$

$$A_n^i = \frac{2Q_i\left[\sin\left(\frac{(2y_i + d_i)}{2}\delta_n\right) - \sin\left(\frac{(2y_i - d_i)}{2}\delta_n\right)\right]}{abd_i k_1 \delta_n^2 \phi(\lambda_n)} \tag{16}$$

$$A_{mn}^i = \frac{16Q_i \cos(\lambda_m x_i)\sin(\frac{1}{2}\lambda_m c_i)\cos(\delta_n y_i)\sin(\frac{1}{2}\delta_n d_i)}{abc_i d_i k_1 \beta_{m,n}\lambda_m \delta_n \phi(\beta_{m,n})} \tag{17}$$

Figure 8 shows the values of a and b which are the length and the width of the heat sink. In this work, they are equal to that of the MC PCB. c_i and d_i are equal to longitudinal and transversal pitch respectively. Location of each heat source is shown by x_i and y_i. Other terms include

$$\lambda = \frac{m\pi}{a} \tag{18}$$

$$\delta = \frac{n\pi}{b} \tag{19}$$

$$\beta = \sqrt{\lambda^2 + \delta^2} \tag{20}$$

$$\phi(\zeta) = \frac{\zeta \sinh(\zeta t_1) + h_{eff}/k_1 \cosh(\zeta t_1)}{\zeta \cosh(\zeta t_1) + h_{eff}/k_1 \sinh(\zeta t_1)} \tag{21}$$

where ζ is replaced by λ, δ and β. t_1 and k_1 are the thickness and thermal conductivity of the heat sink base plate. Convection coefficient of the heat sink is measured experimentally. The convection coefficient is calculated using the temperature distribution equation for fins [25]:

$$\frac{T_{Fin\ tip} - T_{Ambient}}{T_{Base} - T_{Ambient}} = \frac{1}{\cosh mL + \frac{h}{mk}\sinh mL} \tag{22}$$

$$m = \sqrt{\frac{hP}{kA_c}} \tag{23}$$

$$M = \sqrt{hPkA_c}(T_{Base} - T_{Amb}) \tag{24}$$

where $T_{Fin,tip}$ and T_{Base} are fin tip and heat sink base temperatures, L is fin height, P is fin perimeter and A_c is fin cross section area. By measuring the heat sink base and fin tip temperatures experimentally, h can be estimated. h_{eff} is obtained by algebraically converting the convection coefficient with fin (h) to effective convection coefficient (without fin).

In the thermal design, calculating the maximum junction temperature is the main concern [19]. This occurs first at the innermost LED in the array. If the location of this LED is taken as x and y, the maximum heat sink thermal resistance can be obtained:

$$R_{Heat\ sink} = \frac{T(x,y,0) - T_f}{Q_i} \tag{25}$$

It should be noted that this equation is slightly different than $R_{Heat\ sink}$ presented in [19] as T_f is subtracted from the LED temperature. Moreover, Q_i is thermal power of a single LED and not the sum of all LED powers. This seems to be missing in the equation presented in [19].

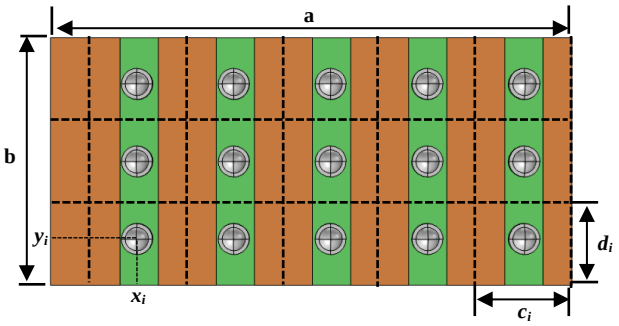

Figure 8 Schematic drawing of the MC PCB showing eccentric heat sources.

Numerical modeling of the LED module

Numerical modeling is performed using the commercial FEA software COMSOL®. A 3D model using the dimensions and thermal properties mentioned in the previous sections is built. Figure 9a shows the geometry of a LED package based on the size and properties mentioned in Table 1. Encapsulation is not modeled separately and is considered as a part of LED lens because it has the same thermal conductivity as the lens. Figure 9b shows the 3D model of the LED module. Due to symmetry, only half of the LED module has been modeled. Moreover, heat sink is not modeled here and instead, the

effective value of convection coefficient (h_{eff}) is calculated by the analytical model and used as a boundary condition on the heat sink base plate. All other surfaces are thermally insulated. To simulate the conditions occurring in the case of the MC PCB without a heat sink, another model without the heat sink base plate is also developed which can be observed in Figure 2a.

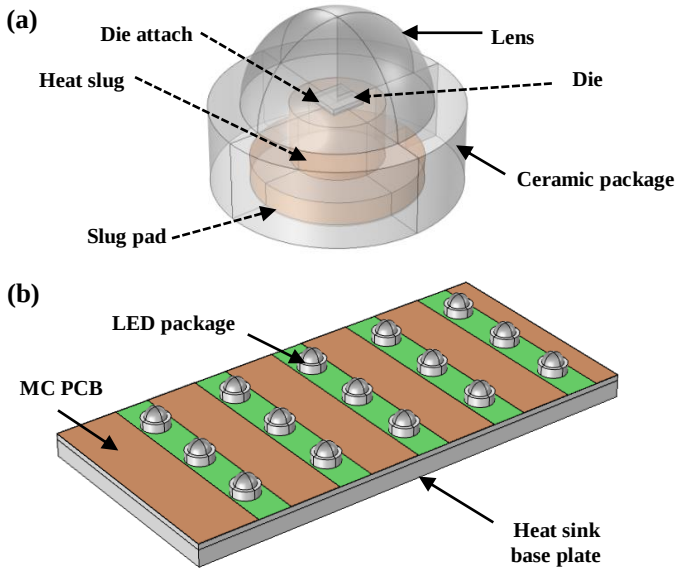

Figure 9 a) Transparent 3D geometry of the LED package in the numerical modeling(dash lines are used to show the hidden objects) b) LED module with the heat sink base plate

RESULTS AND DISCUSSION

LED module thermal performance

Figure 10 shows the temperature profile of the LED module both experimentally by IR imaging and numerically. Ambient temperature in both numerical and experimental studies is 23 ^{o}C based the measured laboratory ambient temperature. Experimental results of the tests on the heat sink show that the convection coefficient (h) is 7 W/m^2 K. Effective convection coefficient (h_{eff}) is calculated based on the heats sink fin dimensions and is equal to 67 W/m^2 K. This value is used as the boundary condition on the backside of the heat sink base plate in the numerical modeling. But for the case of the MC PCB without heat sink, the convection coefficient (h=7 W/m^2 K) is used as the boundary condition.

As can be seen in Figure 10b, the maximum temperature occurs at the die surface and is around 60 ^{o}C whereas the maximum measured temperature in the IR image is 47.7 ^{o}C (Figure 10a). This shows that the die temperature cannot be measured directly from the IR imaging due to the temperature loss in the lens and encapsulation. It can also be observed that the temperature variation between the copper layer conductors and the dielectric layers is very small (less than 1 ^{o}C). This shows that neglecting the copper layers in the analytical model is a valid assumption.

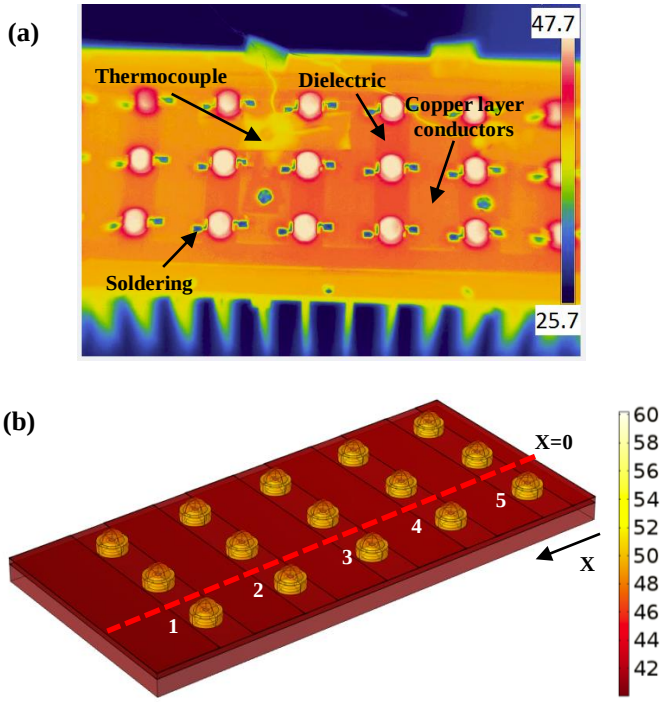

Figure 10 a) IR image of the MC PCB b) temperature profile of the LED module

PCB surface temperature

Figure 11 shows the MC PCB surface temperature profile along the line identified in Figure 10b from the MC PCB mid-plane (x=0) to the edge. Experimental results show that the temperature is relatively uniform when the heat sink is attached and the temperature decrease from the MC PCB center to the edge is less than 2 ^{o}C. However, the temperature profile on the MC PCB without the heat sink is less uniform, showing a temperature drop of around 10 ^{o}C. This shows the role of the heat sink to provide a uniform heat extraction means. Numerical and analytical results are in good agreement with the experimental results especially in the case of MC PCB with heat sink. It should be noted that the analytical models provide the MC PCB temperature only right under the LEDs (maximum thermal resistance). Therefore, the current analytical result is the temperature on the heat sink base plate surface. This temperature is chosen as the MC PCB uncovered surface temperature due to very small temperature difference between this temperature and that of the MC PCB surface in locations without LED (less than 0.5 ^{o}C) based on numerical results. For the case of MC PCB without heat sink, the temperature at the MC PCB backside is calculated by an energy balance. While the temperature drop towards the edges can be observed in the numerical results, the trend cannot be seen in the analytical results because only the maximum temperature is shown here. However, the variations in the analytical results are very small and not significant.

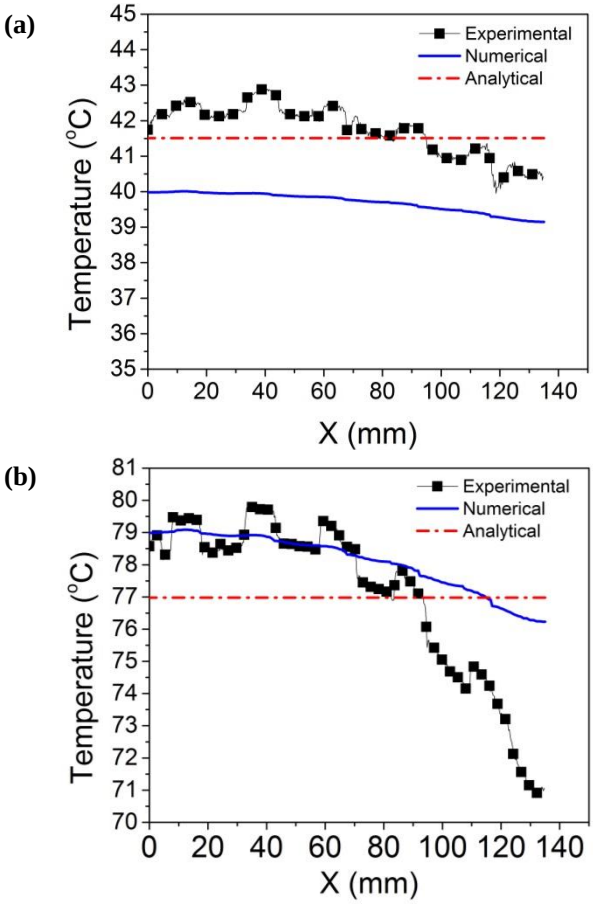

Figure 11 a) MC PCB surface temperature for a complete module (with heats sink) b) MC PCB without heat sink.

MC PCB temperature under LEDs

The MC PCB surface temperature under 5 LEDs can be seen in Figure 12 for two cases of complete module with heat sink and MC PCB without heat sink. The LEDs are the lower row on the MC PCB shown in Figure 10b with their corresponding numbers. It can be seen that the analytical and numerical results are in good agreement. The difference between the MC PCB temperature under the LEDs and that of the visible MC PCB (Figure 11) is approximately 10 °C. This shows the very low spreading capacity of the dielectric layer and hence, its high thermal resistance.

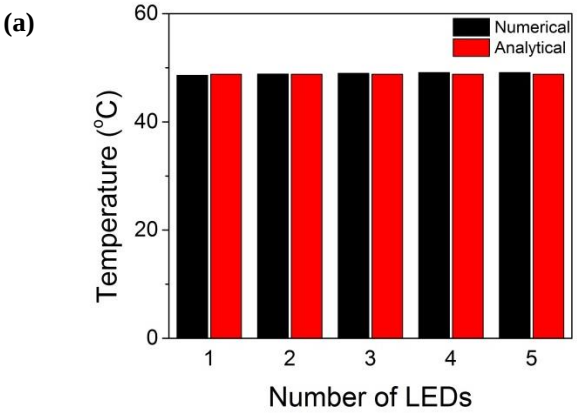

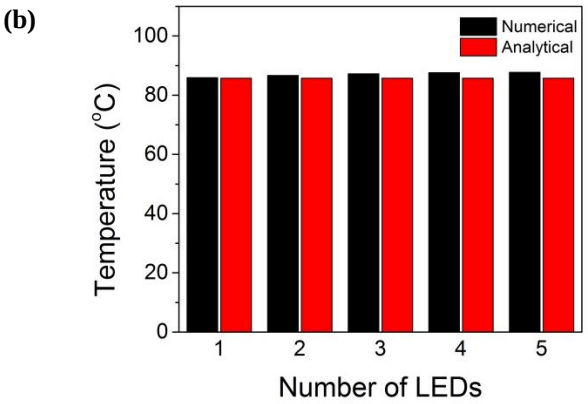

Figure 12 a) MC PCB surface temperature under 5 LEDs for a complete module (with heat sink) b) MC PCB without heat sink.

Die temperature

The die temperature of the LED module for 5 LEDs in the lower row on the MC PCB is shown in Figure 13. As can be seen, the analytical results are consistent with the numerical results and the predicted junction temperatures are very close. The numerical junction temperatures increase gradually form edge to MC PCB center due to higher available space for thermal spreading at the edge compared with the center. The junction temperature of the MC PCB alone is approximately 35 °C higher than the MC PCB with heat sink.

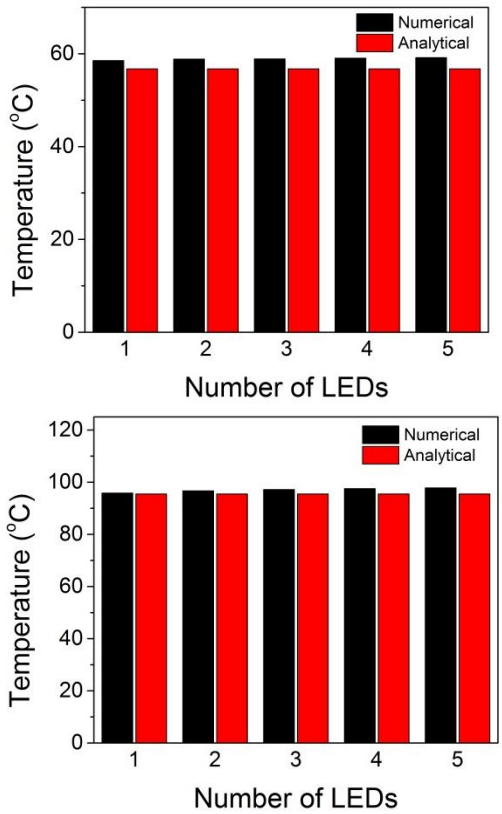

Figure 13 a) Die temperature for a complete module (with heats sink) b) die temperature for MC PCB without heat sink.

Thermal resistance of different components

Using the analytical models, the thermal resistance of each component of the LED module is calculated and showed in Table 2. It can be seen that using the simplified equation for the LED package thermal resistance leads to less than 6% error compared with the value provided by the manufacturer (12 ^{o}C/W). Moreover, the dominant thermal resistance is the heat sink comprising more than 50% of the total thermal resistance. This is mainly due to very low value of natural convection coefficient. LED package and MC PCB each correspond to 25% of the total thermal resistance. MC PCB thermal resistance is mostly caused by the very low thermal conductivity of the dielectric layer while LED package thermal resistance is caused by low thermal conductivity of the die and die attach materials.

Table 2 Thermal resistance of the LED module components (^{o}C/W)

	LED package	MC PCB	Heat sink	Total
Complete module (with heat sink)	11.3	11.9	25	48.9
MC PCB without heat sink	11.3	11.9	-	-

CONCLUSION

A commercial LED module including LED packages, MC PCB and heat sink has been investigated from the thermal point of view. Experimental approaches along with numerical and analytical methods are used to present a thermal resistance model for this LED module. The following conclusions can be drawn from this study:

1- Analytical and numerical models can predict the thermal performance of the LED module provided that all the component dimensions and material thermal conductivities are available.
2- The major thermal resistance in the thermal circuit is the heat sink accounting for more than 50% of the total thermal resistance. This is mainly due to the low natural convection coefficient. MC PCB and LED package each share 25% of the total thermal resistance. This shows that efforts to decrease the total thermal resistance should be more focused on increasing the convection coefficient in the heat sink and decreasing the spreading thermal resistance in the MC PCB.

ACKNOWLEDEMENTS

This research was funded by the ENGAGE program of NSERC and in-kind contributions of LEDTECH.

REFERENCES

[1] Lasance, C., and Poppe, A., 2013, "Thermal management for LED applications," Springer, New York.

[2] Fan, A., Bonner, R., Sharratt, S., 2012, "An innovative passive cooling method for high performance light-emitting diodes," 2012 IEEE/CPMT 28th Semiconductor Thermal Measurement & Management Symposium (SEMI-THERM), USA, pp. 319-24.

[3] Huaiyu, Y., Koh, S., van Zeijl, H., 2011, "A Review of Passive Thermal Management of LED Module," Journal of Semiconductors, **32**(1) pp. 014008 (4 pp.).

[4] Zhang, J., Niu, P., Gao, D., 2012, "Research progress on packaging thermal management techniques of high power LED," 2011 International Conference on Energy, Environment and Sustainable Development, ICEESD 2011, October 21, 2011 - October 23, Trans Tech Publications, Shanghai, China, **347-353,** pp. 3989-3994.

[5] Vipradas, A., Takawale, A., Tripathi, S., 2012, "A parametric study of a typical high power LED package to enhance overall thermal performance," 2012 13th IEEE Intersociety Conference on Thermal and Thermomechanical Phenomena in Electronic Systems, USA, pp. 308-13.

[6] Juntunen, E., Tapaninen, O., Sitomaniemi, A., 2014, "Copper-Core MCPCB with Thermal Vias for High-Power COB LED Modules," IEEE Transactions on Power Electronics, **29**(3) pp. 1410-17.

[7] Maaspuro, M., and Tuominen, A., 2013, "Thermal Analysis of LED Spot Lighting Device Operating in External Natural Or Forced Heat Convection," Microelectronics Reliability, **53**(3) pp. 428-34.

[8] Chien-Ping Wang, Shung-Wen Kang, Kuan-Min Lin, 2014, "Analysis of Thermal Resistance Characteristics of Power LED Module," IEEE Transactions on Electron Devices, **61**(1) pp. 105-9.

[9] Jayawardena, A., Yi-wei Liu, and Narendran, N., 2013, "Analysis of Three Different Junction Temperature Estimation Methods for AC LEDs," Solid-State Electronics, **86**pp. 11-16.

[10] Pardo, B., Gasse, A., Fargeix, A., 2012, "Thermal resistance investigations on new leadframe-based LED packages and boards," 2012 13th International Conference on Thermal, Mechanical and Multi-Physics Simulation and Experiments in Microelectronics and Microsystems, USA, pp. 9 pp.

[11] Han-Kuei Fu, Chien-Ping Wang, Hsin-Chien Chiang, 2013, "Evaluation of Temperature Distribution of LED Module," Microelectronics Reliability, **53**(4) pp. 554-9.

[12] Yung, K. C., Liem, H., Choy, H. S., 2014, "Thermal Investigation of a High Brightness LED Array Package Assembly for various Placement Algorithms," Applied Thermal Engineering, **63**(1) pp. 105-118.

[13] Huang, P., Pan, K., Wang, S., 2012, "Study on packaging structure of high power multi-chip LED," 2012 13th International Conference on Electronic Packaging Technology & High Density Packaging (ICEPT-HDP), USA, pp. 1516-20.

[14] Bender, V. C., Iaronka, O., and Marchesan, T. B., 2013, "Study on the thermal performance of LED luminaire using finite element method," IECON 2013 - 39th Annual Conference of the IEEE Industrial Electronics Society (IECON 2013), USA, pp. 6099-104.

[15] Luo, X., Mao, Z., Liu, J., 2011, "An Analytical Thermal Resistance Model for Calculating Mean Die Temperature of a Typical BGA Packaging," Thermochimica Acta, **512**(1-2) pp. 208-216.

[16] Yu, J., Lu, J., Tong, Y., 2013, "Thermal Analysis of Light Emitting Diode Integrated Light Source Based on a Fourier Series Solution," IEEE Transactions on Components, Packaging and Manufacturing Technology, **3**(4) pp. 612-16.

[17] Cheng, T., Luo, X., Huang, S., 2010, "Thermal Analysis and Optimization of Multiple LED Packaging Based on a General Analytical Solution," International Journal of Thermal Sciences, **49**(1) pp. 196-201.

[18] Xiong, W., Cheng, T., Luo, X., 2009, "Temperature Estimation of High-Power Light Emitting Diode Street Lamp by a Multi-Chip Analytical Solution," IET Optoelectronics, **3**(5) pp. 225-32.

[19] Ha, M., and Graham, S., 2012, "Development of a Thermal Resistance Model for Chip-on-Board Packaging of High Power LED Arrays," Microelectronics Reliability, **52**(5) pp. 836-844.

[20] Corfa, A., Gasse, A., Bernabe, S., 2010, "Analytical and FEM simulations of the thermal spreading effect in LED modules and IR thermography validation," Conference on Thermal, Mechanical & Multi-Physics Simulation and Experiments in Microelectronics and Microsystems (EuroSimE 2010), USA, pp. 8.

[21] Harris, J., and Matthews, M., 2009, "Selecting Die Attach Technology for High-Power Applications," **2014**(13/04/2014).

[22] Bridgelux, 2011, "Bridgelux BXCE 45x45 NLX-5 Product Data Sheet DS-C10," **2014**(09/04/2014).

[23] Sarvar, F., Poole, N. J., and Witting, P. A., 1990, "PCB Glass-Fibre Laminates: Thermal Conductivity Measurements and their Effect on Simulation," Journal of Electronic Materials, **19**(12) pp. 1345-50.

[24] Muzychka, Y. S., Culham, J. R., and Yovanovich, M. M., 2003, "Thermal Spreading Resistance of Eccentric Heat Sources on Rectangular Flux Channels," Transactions of the ASME.Journal of Electronic Packaging, **125**(2) pp. 178-85.

[25] Bergman, T.L., Lavine, A.S., Incropera, F.P., 2011, "Fundamentals of Heat and Mass Transfer," Wiley, USA, pp. 1048.